Stress and structure of $c(2\times2)$ and $p2gg(4\times2)$ Mn/Cu(001) surface alloys

W. Pan,[1,2,*] R. Popescu,[1] H. L. Meyerheim,[1] D. Sander,[1] O. Robach,[3] S. Ferrer,[3] Minn-Tsong Lin,[2,4,†] and J. Kirschner[1]
[1]*Max-Planck-Institut für Mikrostrukturphysik, Weinberg 2, D-06120 Halle, Germany*
[2]*Department of Physics, National Taiwan University, Taipei 106, Taiwan*
[3]*European Synchrotron Radiation Facility (ESRF), Boîte Postale 220, F-38043 Grenoble, France*
[4]*Institute of Atomic and Molecular Sciences, Academia Sinica, Taipei 106, Taiwan*
(Received 16 February 2004; revised manuscript received 3 August 2004; published 31 May 2005)

We present a combined *in situ* surface stress and structural study of MnCu surface alloys formed by deposition of Mn on Cu(001) at 300 and 420 K. Mn-induced surface alloying induces a compressive stress change, which grows in proportion to the Mn coverage up to 0.5 monolayers (ML), where it reaches −1.2 N/m (1 ML: 1.5×10^{15} atoms cm^{-2}). This stress is related to the formation of the $c(2\times2)$ surface alloy. No further alloying is observed upon subsequent Mn deposition at 300 K, at 420 K the formation of the $p2gg(4\times2)$ Mn-Cu alloy occurs, and a compressive stress change of −2.3 N/m at 1.3 ML is found. Surface x-ray-diffraction analysis of the two-layer alloy $p2gg$-(4×2)-phase indicates an amplitude of 0.9 Å for vertical buckling and lateral modulations of the atomic positions, the latter leading to the doubling of the lattice constant as compared to the $c(2\times2)$ structure. Evidence for a compositional gradient within the alloy structure is given, where the Mn concentration is above and below 50% in the topmost and second alloy layer, respectively. The importance of surface stress relief and Mn/Cu atomic size mismatch for the Mn-induced surface stress change is discussed.

DOI: 10.1103/PhysRevB.71.174439 PACS number(s): 68.35.Gy, 68.35.Ct, 68.55.−a

I. INTRODUCTION

The geometrical structure of surfaces and interfaces plays an important role for the physical properties of epitaxial film systems. Instructive examples where tiny modifications of the atomic arrangement have decisive consequences on the physical properties are film growth mode, magnetic interface anisotropy, interlayer exchange (bias) coupling, and spin-dependent transport phenomena.[1–4] Besides epitaxial growth, often the formation of surface alloys is observed, even in cases where the elements are immiscible in the bulk.[5] The impact of surface alloy formation on the physical properties of an ultrathin film in the thickness range of a few atomic layers can be quite significant.

Mn on Cu(001) is a prototype surface alloy, and depending on the preparation conditions, various long-range-ordered superstructures were observed and investigated by low-energy electron diffraction (LEED).[6] Deposition of more than 0.3 monolayers (ML) Mn on Cu(001) above 270 K leads to the formation of a $c(2\times2)$ LEED pattern (1 ML is defined as 1 ad-atom per surface Cu atom corresponding to 1.5×10^{15} atoms cm^{-2}). At 420 K, a $p2gg(4\times2)$ LEED pattern is observed for Mn deposition in excess of 1 ML.[6,7]

For both superstructures, the formation of a surface alloy by direct Mn-Cu atomic exchange was proposed, i.e., Mn atoms are incorporated into the Cu surface, where they replace Cu surface atoms.[8–11] Scanning tunneling microscopy (STM) studies also contributed to the determination of the atomic arrangements in the $c(2\times2)$ and $p2gg(4\times2)$ structures.[7,9,12–14] The $c(2\times2)$ structure is characterized by an ordered MnCu surface alloy,[12,14] where every other surface Cu atom is replaced by Mn. Similarly, the $p2gg(4\times2)$ pattern was also attributed to an ordered MnCu alloy, but—although the detailed atomic arrangement has not been identified so far—the alloy was proposed to extend over the topmost two layers.[6,7]

This work combines highly sensitive stress measurements with a surface x-ray-diffraction (SXRD) structure determination. The results shed new light on the largely unexplored correlation between general phenomena such as surface alloy formation, surface stress, and structure relaxation of metallic surface layers. Various atomic processes, such as the incorporation of Mn atoms into the Cu substrate, Mn island formation, and de-alloying, are directly related to characteristic stress signatures. The magnitude of the respective stress change is discussed in the context of the geometrical structure. The results indicate that besides atomic size misfit and structural relaxation, relief of tensile surface stress of the clean Cu(001) substrate is decisive for the resulting stress change.

II. EXPERIMENT

Stress measurements were performed by the curvature technique[18] in an ultrahigh-vacuum chamber (UHV) (base pressure: 1×10^{-10} mbar). A Cu(001) crystal cantilever (width: 3 mm, thickness: 124 μm) was clamped at one end to the manipulator to allow free bending. The Cu(001) surface was cleaned by Ar^+ sputtering (1 keV), followed by short annealing to 720 K for 30 s. Surface cleanliness was checked by Auger electron spectroscopy (AES) (surface contaminants <1% of a ML) and sharp diffraction spots were obtained by LEED.

Stress measurements were carried out during Mn deposition at 300 and 420 K. The sample temperature was calibrated by thermocouples attached to a dummy sample. The change of surface stress, $\Delta\tau_s$, is derived from the change of curvature of the crystal, $\Delta(1/R)$, using the relation $\Delta\tau_s$

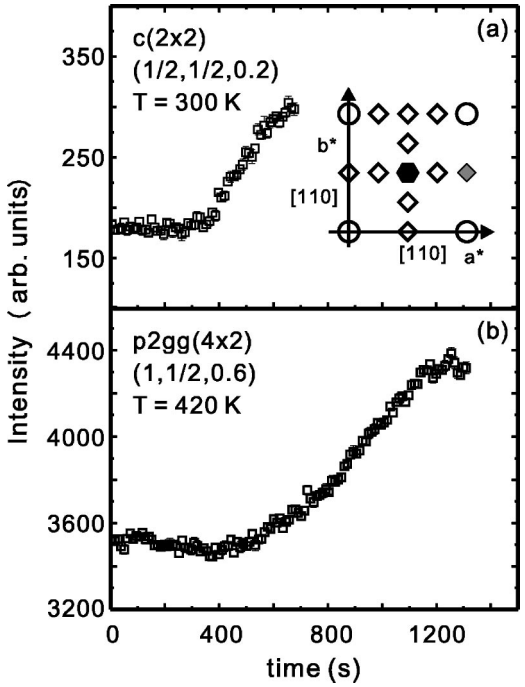

FIG. 1. Deposition time dependence of the $(1/2,1/2)$ (a) and $(1,1/2)$ (b) superstructure reflection intensities characteristic of the $c(2\times2)$ and the $p2gg(4\times2)$ structure. The inset in (a) shows a sketch of the reciprocal lattice in the a^*-b^* plane. Circles represent Cu(001) crystal truncation rods. Diamonds indicate reflections related to the $p2gg(4\times2)$ superstructure. The hexagon marks the $(1/2,1/2)$ rod related to the $c(2\times2)$ superstructure below 0.5 ML.

$=\Delta(\tau_f t_f)=[Y t_s^2/6(1-\nu)]\times\Delta(1/R)$, where t_f and t_s are the thickness of the film (Mn) and the substrate (Cu), respectively. Y (Cu: 66.7 GPa) and ν (Cu: 0.42) are the Young modulus and the Poisson ratio, and R is the radius of curvature.[15,16] Film stress (τ_f) is derived from the slope of the curvature signal as a function of film thickness.[18]

SXRD experiments were carried out at the beamline ID3 of the European Synchrotron Radiation Facility (ESRF) in Grenoble. The Cu crystal (diameter: 10 mm, thickness: 3 mm) was prepared as outlined above.[17]

In all experiments, Mn was deposited by thermal evaporation from a Mn rod (99.5 at. %). Coverage and deposition rate were checked by AES, and by monitoring the intensity of characteristic superlattice reflections related to the $c(2\times2)$ and the $p2gg(4\times2)$ structure with SXRD.[6,7]

Figure 1 shows reflection intensities measured at the $(1/2,1/2)$ and the $(1,1/2)$ superlattice rods as a function of the deposition time. The appearance of these reflections indicates the formation of the $c(2\times2)$ and the $p2gg(4\times2)$ structure, respectively.[19] The inset in (a) shows the symmetry-independent part of the reciprocal lattice in the a^*-b^* plane.[20] Open circles represent the rods of integer order, while the diamonds correspond to superlattice rods related to the $p2gg(4\times2)$ structure. The black hexagon indicates the $(1/2\ 1/2)$ rod characteristic of the $c(2\times2)$ structure for a Mn coverage below 0.5 ML. The reflection intensities saturate after about 600 $[c(2\times2)]$ and 1200 s $[p2gg(4\times2)]$, indicating a factor 2 difference in the total Mn coverage between the respective superstructures.

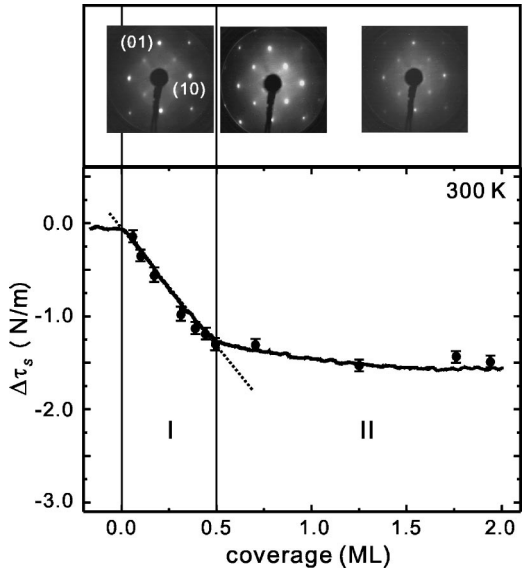

FIG. 2. Surface stress change, $\Delta\tau_s$, and LEED patterns observed during Mn deposition at 300 K. Filled circles represent individual measurements; the solid line corresponds to one measurement during the deposition of 2 ML. LEED images (E=112 eV) were taken at 0.3, 0.5, and 1.75 ML. The dashed line emphasizes the linear stress-coverage dependence up to "kink" in the stress curve.

A SXRD structure analysis was carried out for the $p2gg(4\times2)$ superstructure. In total, 512 reflections were measured and subsequently reduced to 285 independent reflections after averaging over symmetry-equivalent reflections. Structure factor intensities $|F(hkl)|^2$ were derived from the integrated intensities and corrected for geometrical factors.[23] Standard deviations (σ) of the $|F(hkl)|^2$ values were calculated from the counting statistics and the reproducibility of symmetry-equivalent reflections.[21,22]

III. RESULTS

A. Stress behavior of Mn on Cu(001) at 300 K

Stress measurements during deposition of Mn on Cu(001) at 300 K are shown in Fig. 2. The continuous curve is measured during the deposition of 2.0 ML Mn. The individual data points represent the measured surface stress change at smaller coverage. The surface stress change, $\Delta\tau_s$, is compressive (negative signal). It amounts to -1.2 N/m at 0.5 ML, and levels off at -1.4 N/m for 2 ML. An obvious "kink" in the slope of the stress curve is found at 0.5 ML, which separates the curve into two regimes: a compressive regime (I) below 0.5 ML, where the stress increases in proportion to the Mn coverage, and an almost stress-free state (II) at larger coverage.

LEED patterns for 0.3, 0.5, and 1.75 ML Mn are shown in the upper panel of Fig. 2. For a Mn coverage above 0.3 ML, $c(2\times2)$ diffraction spots are observed, and their intensity saturates at 0.5 ML. The background intensity of the LEED pattern increases at larger coverage.

The superstructure spots indicate that the formation of the long-range-ordered $c(2\times2)$ surface alloy already starts at

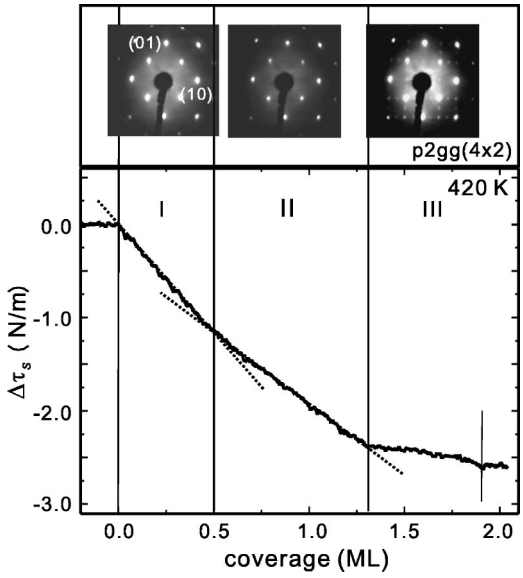

FIG. 3. Surface stress change $\Delta\tau_s$ during deposition of Mn on Cu(001) at 420 K and LEED images (E=112 eV) at 0.5, 1.2, and 1.7 ML.

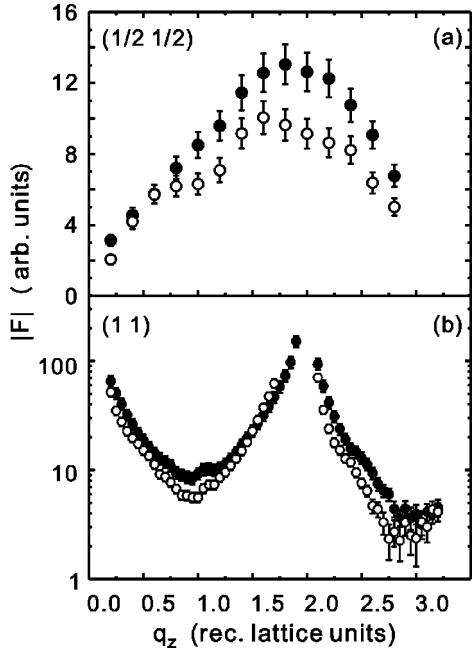

FIG. 4. SXRD intensities along the (0.5, 0.5) (a) and the (1,1) (b) rod for the $c(2\times2)$ (filled symbols ●) and for the $p2gg(4\times2)$ structure (open symbols ○).

0.3 ML. Similarly, in the SXRD data [see Fig. 1(a)] the $(1/2,1/2)$ reflection intensity starts to increase above background after 400 s. Since the saturation at 600 s is related to 0.5 ML Mn, where the $c(2\times2)$ structure is completely formed, this corresponds to about 1/3 ML. In summary, both LEED and SXRD indicate that long-range ordering of the $c(2\times2)$ superstructure starts at about 1/3 ML, but stress experiments clearly indicate that alloying-induced stress change sets in from the very beginning of Mn deposition.

B. Stress behavior of Mn on Cu(001) at 420 K

The surface stress change, $\Delta\tau_s$, during deposition of Mn on Cu(001) at 420 K is shown in Fig. 3. We divide the coverage range into three regimes—(I), (II), and (III)—to indicate the different slopes of the stress curve as a function of Mn coverage. In regime (I), the compressive surface stress change increases in proportion to the Mn coverage up to 0.5 ML Mn, where the first kink of the stress curve is observed. In regime (II), a continuation of compressive stress, albeit with reduced slope, is found. A second kink in the stress curve at −2.3 N/m for 1.3 ML Mn marks the transition to regime (III). In regime (III), no further significant stress change is measured.

The corresponding LEED patterns are shown in the upper panel of Fig. 3. A $c(2\times2)$ LEED pattern is observed for regimes (I) and (II), and a $p2gg(4\times2)$ pattern[7] is found in regime (III).

In regime (I), the Mn-induced change of surface stress and the LEED pattern is identical to that observed for Mn deposition at 300 K. In contrast, at 420 K there is a continued increase of compressive stress in regime (II), which is not observed at 300 K. It is related to the formation of the $p2gg(4\times2)$ structure. SXRD data shown in Fig. 1(b), where the $(1,1/2,0.6)$ reflection intensity is plotted versus deposition time, indicate an intensity onset after about 700 s. This corresponds to 2/3 ML. We conclude that the formation of the $p2gg(4\times2)$ structure starts directly after completion of the $c(2\times2)$ structure.

Structure models for the $c(2\times2)$ and the $p2gg(4\times2)$ structures were proposed in Refs. 6, 7, and 14. While the atomic geometry of the $c(2\times2)$ structure is well established, no details for the $p2gg(4\times2)$ structure have been presented so far, but will be discussed below.

C. X-ray-diffraction structure analysis of the $p2gg(4\times2)$ structure

Figure 4 shows in (a) the diffracted intensities along the $(1/2,1/2)$ superlatttice rod, and in (b) along the (1,1) crystal truncation rod for both the $c(2\times2)$ structure (filled symbols) and the $p2gg(4\times2)$ structure (open symbols). The measurements show an obvious similarity of the intensity distribution along the rods for both structures, which suggests a similar atomic structure.

The c-projected Patterson function $P(u,v)$ is calculated from the in-plane structure factor intensities, $|F(hk0)|^2$, according to $P(u,v)=\Sigma|F(hk0)|^2\times\cos[2\pi(hu+kv)]$, where the summation runs over all $(hk0)$ reflections.[24] Maxima in $P(u,v)$ are related to interatomic vectors, and their intensity is proportional to the multiplicity of the vector within the unit cell and to the product of the atomic numbers of the respective atom pair.[25]

Figure 5 shows $P(u,v)$ calculated from 14 in-plane reflections. Within the asymmetric unit (dashed rectangle), five strong maxima are observed and labeled 1 to 5. For direct comparison, a schematic model of the fcc Cu(001) surface is shown on the same scale in the lower part of the figure.

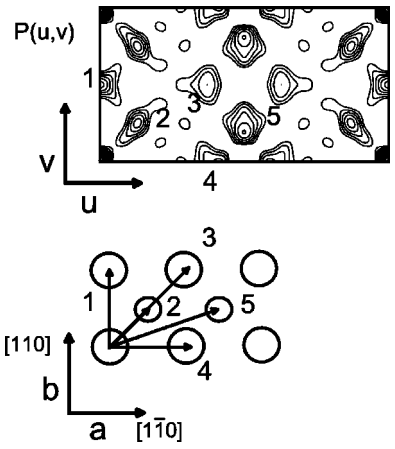

FIG. 5. Two-dimensional Patterson function, $P(u,v)$, for the $p2gg(4\times2)$ structure. Maxima labeled by 1–5 correspond to interatomic vectors. The dotted rectangle indicates the asymmetric unit. Two fcc-Cu(001) surface unit cells including the top (large circles) and second layer (small circles) are shown in the lower part. Arrows indicate interatomic vectors and are labeled corresponding to the maxima in $P(u,v)$.

Along the *a* axis, corresponding to the $[1\bar{1}0]$ direction in bulk Cu, two unit cells are displayed. Large and small circles correspond to atoms in the top and second layers, respectively.

Peaks 1 and 2 can be attributed to correlations between atoms within the top (No. 1) and between the top and second layer (No. 2). There is direct evidence for alloying, because peak 1 corresponds exactly to a bulk interatomic vector and it would not be observed without the presence of chemical contrast. On the other hand, maxima 3, 4, and 5 do not directly match the interatomic vectors of the bulk-terminated structure. Instead, these maxima indicate larger interatomic distances, i.e., the corresponding atoms are laterally shifted. From this result, it is tempting to assume that the doubling of the size of the surface unit cell along $[1\bar{1}0]$ is due to shifts of the atoms out of the bulk in-plane positions, which they occupy in the $c(2\times2)$ structure. In addition, vertical relaxations and changes in the Mn concentration as compared to the $c(2\times2)$ structure, including a second alloy layer, are considered in a starting model for the structure refinement.

The structure analysis was carried out by least-square fitting of calculated intensities derived from the structure model to the measured intensities. Figure 6 shows the experimental intensities on a logarithmic scale as solid symbols. Reflections are indexed according to the primitive (1×1) unit cell. Both integer order truncation rods (CTR's) and fractional order superlattice rods were simultaneously used for the refinement, but allowing for different scale factors for each subset of data. The solid lines represent the best fit characterized by an unweighted residual $[R_u(I)]$ of 0.097 and a goodness of fit (GOF) of 0.88.[26]

The refined structure model is shown in Fig. 7 in top view (a), and in a perspective side view (b). Pink and green balls represent Mn and Cu atoms, respectively. Only the top two layers are shown, since consideration of deeper layers in the data analysis did not improve the fit. In general, the atomic

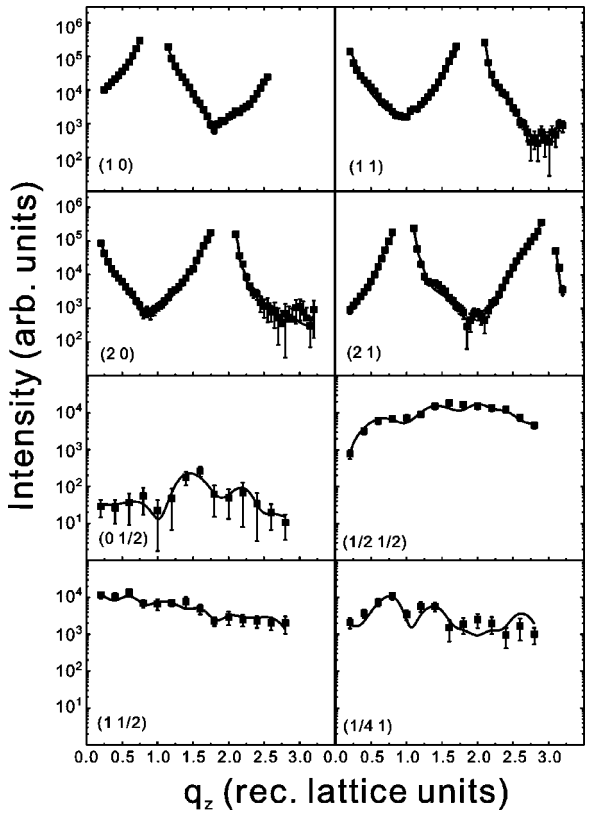

FIG. 6. Experimental (symbols) and calculated (lines) intensities for the $p2gg(4\times2)$ Mn/Cu(001) structure. The corresponding structure model is shown in Fig. 7.

positions can be occupied by both species, and this reflects chemical disorder. This is taken into account in the calculations by coherent averaging using a fractional occupancy of the atomic sites by Cu and Mn. In Fig. 7, this is represented by hemispheres representing Mn and Cu at the same site. Due to the similar atomic numbers of Mn and Cu ($Z=25$ and 29), their atomic scattering factors differ by only 15–20 % over the experimentally accessible *k*-space range, which complicates the chemical identification. Before we discuss the Mn concentration within the different layers, we first consider the atomic positions.

In Fig. 7(a), the dotted rectangle represents the (4×2) unit cell. In the top layer, two symmetrically independent sites are occupied. These are close to the bulk-terminated positions at $(x,y)=(1/8,1/4)$ labeled (α) and $(3/8,1/4)$ labeled (β) within the surface unit cell. The basic characteristics of the structure are lateral shifts of the atoms out of the bulk positions. In this way, a wavelike modulation pattern is formed as indicated by the dotted lines. The modulation amplitude is about 0.4 Å (the error bar for the distance determination is in the 0.10–0.15 Å range). The atomic shifts induce a doubling of the lattice constant along $[1\bar{1}0]$ as compared to the $c(2\times2)$ structure.

Figure 7(b) shows the surface in a perspective view along [100]. Lateral modulations of 0.4 Å are also present along the $\langle100\rangle$ directions and are a direct consequence of the modulation along $\langle110\rangle$. In addition, considerable vertical corrugation is found. Alternate atomic rows are raised verti-

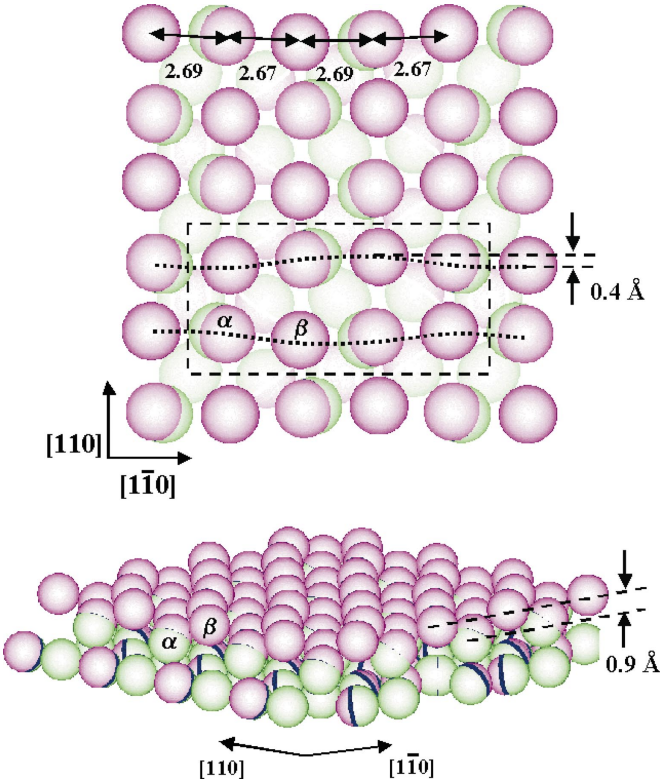

FIG. 7. (Color) Model for the $p2gg(4\times2)$ structure in top view (a) and side view (b) as derived from the SXRD analysis. Pink and green balls represent Mn and Cu atoms, respectively.

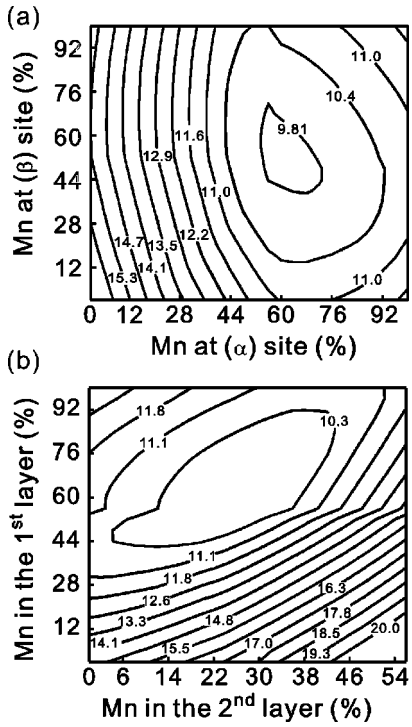

FIG. 8. (a) Contour plot of the unweighted residuum vs Mn concentration in positions α and β. (b) Contour plot of the unweighted residuum vs Mn concentration in the top two layers.

cally by about 0.9 Å. This corrugation is larger than in the $c(2\times2)$ structure, where the Mn atoms are located about 0.3 Å above the surface and no lateral modulation exists.[6,11] The enhanced vertical buckling and the lateral modulation in the $p2gg(4\times2)$ superstructure can be attributed to the larger Mn concentration in the top layer as compared to the $c(2\times2)$ alloy, since the diameter of the Mn atom (γ-Mn: 2.73 Å) (Ref. 27) is larger than that of the Cu atom (2.56 Å).[27] We determine interatomic distances between top-layer atoms in the range 2.57–2.97 Å with an average value of 2.73 Å. The nearest-neighbor distances are thus larger than 2.58 Å, which is the Mn-Cu interatomic distance in the $c(2\times2)$ structure.[6,11]

Our structural model provides a straightforward explanation for the STM images of Kraan *et al.*[7] These images indicate bright and dark stripes running along [100], and we identify the stripes with the different atomic rows displayed in Fig. 7(b). Furthermore, the authors find a corrugation between 0.4 and 0.9 Å, depending on the tip conditions. As in the case of STM images of the $c(2\times2)$ structure, only 50% of the atoms are imaged, which is commonly ascribed to the imaging of only Mn atoms.

In the next step of the analysis, the Mn concentration within the first two layers was systematically varied to find the best fit. Figure 8(a) is a contour plot of the unweighted residual, R_u, as a function of the Mn concentration in positions α and β. The total occupancy ($\Theta_{\mathrm{Mn}}+\Theta_{\mathrm{Cu}}$) at each site was set to 100%. There is a pronounced dependence of R_u on the Mn concentration in the α site with a best-fit value at about 65%. For the β site, we find a broad minimum at about 60% leading to a total Mn coverage of 0.6 ML in the top layer. Similarly, in Fig. 8(b), R_u is plotted as a function of the *total* Mn concentration within the top and second layer, respectively. We find a very shallow minimum at about 65% in the top layer and only 30–35 % in the second layer. In total, this adds up to about 0.95 ML coverage, consistent with the amount of Mn necessary to form the $p2gg(4\times2)$ superstructure.

Since the Mn atomic radius is larger than that of Cu, we suggest that the atoms, which stick out of the surface (β), are mainly Mn atoms. The β-site occupation is about 60%, based on the best fit, but the minimum is very broad and values up to 80% are conceivable. While the assignment of Mn concentrations to specific sites is associated with large error bars, the data nevertheless indicate a considerable difference between the Mn concentration in the top and second alloy layer, as displayed in Fig. 8(b). The analysis clearly shows that a Mn concentration above 50% in the top layer and a Mn concentration below 50% in the second layer are preferred.[28]

IV. DISCUSSION

A. Alloying-induced stress in the initial growth

A common stress signature of the $c(2\times2)$ MnCu surface alloy is the compressive surface stress change of −1.2 N/m at 0.5 ML Mn coverage. We propose that the relief of tensile surface stress in the Cu(001) surface induced by alloying with Mn is the key factor determining the Mn-induced surface stress change.

Tensile surface stress reflects the general tendency to lower the interatomic distances between the top-layer atoms as compared to the bulk. In the case of Cu, the interatomic distance is 2.56 Å. Calculations of surface stress of clean Cu(001) indicate a tensile stress of the order of +1.4 to +1.7 N/m.[29]

As a bulk analog for the 50:50 Mn-Cu surface alloy, we chose the random $Mn_{0.48}Cu_{0.52}$ alloy[30] for comparison. In this alloy, the Mn-Cu interatomic distance (2.66 Å) is enhanced by 3.9% as compared to Cu. In the $c(2\times2)$ surface alloy, the Mn-Cu interatomic distances are almost unchanged as compared to Cu (2.58 Å) despite the 0.3 Å vertical Mn buckling. We conclude that the tendency of the surface to adopt a smaller interatomic distance as compared to the bulk applies to the MnCu-alloy system. To illustrate the magnitude of the Mn-induced surface stress change, we may treat the surface layer as a strained film and calculate the resulting stress.[31]

Based on the bulk lattice constant of the random MnCu alloy (3.75 Å), a compressive misfit (η) results: $\eta=(a_{Cu}-a_{MnCu})/(a_{MnCu})=-3.9\%$. Using the biaxial modulus for the random MnCu alloy [91 GPa (Ref. 32)], the calculated misfit-induced stress is −3.5 GPa. This corresponds to a compressive surface stress change of −0.66 N/m, which is only half of the measured value (−1.2 N/m).

Thus, we conclude that the stress induced by lattice strain is not sufficient to explain the large magnitude of the measured stress. The relief of the tensile surface stress of Cu(001) is therefore the decisive factor, which determines the Mn-induced change of surface stress.

For the films grown at 300 K, additional deposition of Mn above 0.5 ML does not induce a new surface structure, nor does it change the stress significantly. We conclude that the expelled Cu atoms and the deposited Mn atoms do not form an ordered MnCu alloy. Such an ongoing alloy formation should have caused a further increase in compressive stress, which is not detected at 300 K but at 420 K.

B. Stress behavior for alloying at larger coverage

Mn deposition at 420 K leads to a more complicated stress behavior. The resulting stress below 0.5 ML [regime (I) of Fig. 5] is attributed to the $c(2\times2)$ MnCu surface alloy formation as discussed above. In regime (II), between 0.5 and 1.3 ML, we observe an ongoing linear increase of the compressive stress with Mn deposition. The slope of the stress curve in regime (II), where the $p2gg(4\times2)$ structure forms, is *smaller* than that in regime (I). The SXRD analysis of the $p2gg(4\times2)$ structure indicates considerable geometrical and compositional reorganization.

The most important result of the structure analysis of the $p2gg(4\times2)$ structure is substantial in-plane and out-of-plane buckling. In addition, a composition gradient is determined within the alloy. The Mn concentration is above and below 50% in the top and second layers, respectively.

We limit the discussion of the resulting stress change to two important aspects: Why does the compressive stress continue to increase for depositions in excess of 0.5 ML Mn, and why does it do so with a reduced slope as compared to regime (I)? A top-layer Mn concentration above 50% changes the local bonding stoichiometry as compared to the $c(2\times2)$ structure. In the latter, every other Cu atom is replaced by Mn, and Cu-Mn bonds are formed. A larger Mn concentration leads to Mn atoms in nearest-neighbor positions, and Mn-Mn bonds will be formed in consequence. If we assume for simplicity that the Mn-induced relief of the tensile surface stress of clean Cu(001) has been largely completed for a concentration of 50%, then it seems plausible that the incorporation of additional Mn atoms into the surface layer induces an even larger compressive stress, due to the larger atomic size of Mn as compared to Cu. Thus, we tentatively attribute the continued increase of the compressive stress upon Mn deposition in regime (II) to the Mn-induced lattice distortion in the topmost layer. This picture fundamentally differs from the mechanism made responsible for the compressive stress in regime (I), where relief of tensile surface stress was inferred.

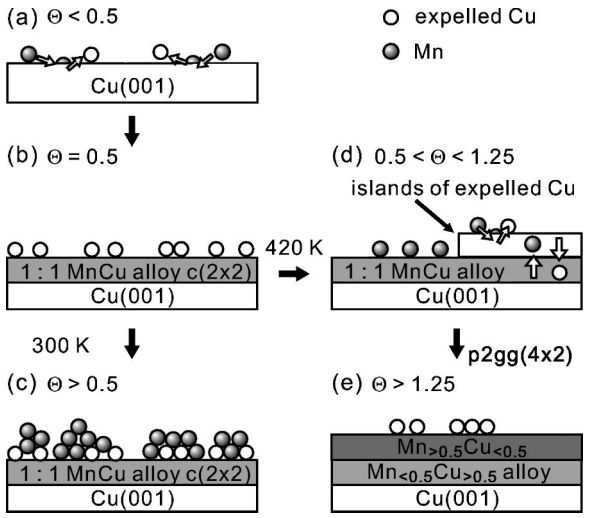

FIG. 9. Schematic model of MnCu surface alloy formation. Left [(a)–(c)] and right [(d),(e)] panels show the evolution of the structure at 300 and 420 K, respectively. At 300 K, only one $c(2\times2)$ alloy layer forms; additional Mn deposition does not lead to further growth of an ordered structure. At 420 K, a two-layer alloy is formed. Interlayer Mn-Cu exchange processes lead to a compositional gradient characterized by a Mn concentration above and below 50% in the topmost and second alloy layers, respectively.

The coverage- and temperature-dependent evolution of the MnCu surface alloy structures is schematically summarized in Fig. 9. Left [(a)–(c)] and right [(d),(e)] panels refer to $T=300$ and 420 K, respectively. While for 300 K no further alloy growth beyond 0.5 ML coverage is observed, the right panels of Fig. 9 illustrate that at 420 K, continued alloy formation takes place. In the beginning, this proceeds by the same atomic exchange mechanism as in the case of the $c(2\times2)$ structure, but continued Mn deposition beyond 0.5 ML does not lead to the growth of a second $c(2\times2)$ layer on the previously formed one. We speculate that this is due to increasing stress and the repulsive forces between Mn atoms in different layers.

Based on the SXRD analysis, we propose a growth mechanism involving *de-alloying* of the second layer, which

is mediated by an interlayer atomic exchange mechanism, where Mn atoms from the second layer are exchanged with Cu atoms in the top layer. This process is symbolized by the vertical arrows in Fig. 9(d). The SXRD data indicate that the Mn concentration in the top layer is enriched to about 60–80 %, while it is depleted to roughly 35% in the second layer.

Enrichment of the top layer by large Mn atoms induces vertical buckling (0.9 Å), much larger than observed (0.3 Å) for the $c(2\times2)$ structure and concomitant the lateral modulations in the $p2gg$-(4×2) reconstruction. These structural relaxations are made responsible for the smaller slope of the stress curve in regime (II) as compared to regime (I).

V. CONCLUSION

Quantitative stress and surface x-ray-diffraction experiments were carried out to study the correlation between surface alloy formation, resulting change of surface stress, and alloying-induced structural relaxation.

Our study relates surface stress changes with structural models for surface alloy phases formed by the deposition of Mn on Cu(001). Growth of the $c(2\times2)$ surface alloy of Mn on Cu(001) at 300 K induces a compressive stress of −1.2 N/m, which is related to Mn-induced relief of tensile surface stress of clean Cu(001). Continued Mn deposition at 420 K leads to the formation of the $p2gg(4\times2)$ phase, which is characterized by a two-layer alloy structure. Top-layer vertical and lateral atomic relaxations are related to Mn enrichment above 50%, while the second layer is depleted to about 35%. These structural relaxations are responsible for the observed reduced slope of the stress versus coverage curve during formation of the $p2gg(4\times2)$ surface structure compared to that observed for the $c(2\times2)$ structure. Our results support the view that the incorporation of larger atoms in a surface layer can reduce the tensile surface stress of the clean surface.[33]

ACKNOWLEDGMENTS

We thank H. Menge for the skillful preparation of the Cu(001) crystal. W. Pan and M.-T. Lin acknowledge the financial support from the National Science Council in Taiwan (Grant No. NSC-92-2112-M-002-028), MOE, and MOEA Program (Grant No. 92-EC-17-A-08-S1-0006), and of the Max Planck Society of Germany.

*Present address: Department of Physics, National Dong-Hwa University, Hua-Lien 974, Taiwan.

†Author to whom correspondence should be addressed. E-mail address: mtlin@phys.ntu.edu.tw

[1] A. M. N. Niklasson, B. Johansson, and H. L. Skriver, Phys. Rev. B **59**, 6373 (1999).

[2] S. Blügel, Appl. Phys. A: Mater. Sci. Process. **63**, 595 (1996).

[3] M.-T. Lin, C. H. Ho, C.-R. Chang, and Y. D. Yao, Phys. Rev. B **63**, 100404(R) (2001).

[4] M.-T. Lin, C. H. Ho, C.-R. Chang, and Y. D. Yao, J. Appl. Phys. **89**, 1 (2001).

[5] J. Tersoff, Phys. Rev. Lett. **74**, 434 (1995).

[6] T. Flores, M. Hansen, and M. Wuttig, Surf. Sci. **279**, 251 (1992).

[7] R. G. P. V. der Kraan and H. V. Kempen, Surf. Sci. **338**, 19 (1995).

[8] M. Wuttig, B. Feldmann, and T. Flores, Surf. Sci. **331–333**, 659 (1995).

[9] T. Flores, S. Junghans, and M. Wuttig, Surf. Sci. **371**, 1 (1997).

[10] H. Ibach, M. Giesen, T. Flores, M. Wuttig, and G. Treglia, Surf. Sci. **364**, 453 (1996).

[11] R. Popescu, H. L. Meyerheim, D. Sander, A. Ernst, O. Robach, S. Ferrer, and J. Kirschner (unpublished).

[12] M. Wuttig, S. Junghans, T. Flores, and S. Blügel, Phys. Rev. B **53**, 7551 (1996).

[13] T. Flores, S. Junghans, and M. Wuttig, Surf. Sci. **371**, 14 (1997).

[14] D. Wortmann, S. Heinze, G. Bihlmayer, and S. Blügel, Phys. Rev. B **62**, 2862 (2000).

[15] H. Ibach, Surf. Sci. Rep. **29**, 193 (1997); **35**, 71(E) (1999).

[16] R. F. S. Hearmon, *The Elastic Constants of Crystals and Other Anisotropic Materials*, Landolt-Börnstein Numerical Data and Functional Relationships in Science and Technology Group III, Vol. 18, supplement to III/11 (Springer, Berlin, 1984), $Y_{Cu}=66.7$ GPa, $\nu_{Cu}=0.42$.

[17] R. Mahesh, D. Sander, S. M. Zharkov, and J. Kirschner, Phys. Rev. B **68**, 045416 (2003).

[18] W. Pan, D. Sander, M.-T. Lin, and J. Kirschner, Phys. Rev. B **68**, 224419 (2003).

[19] D. Sander, Rep. Prog. Phys. **62**, 809 (1999).

[20] We use a sample setting corresponding to a primitive surface unit cell, where the surface (s) setting is related to the face-centered-cubic setting of the bulk (b) by the following relations: $[100]_s=1/2\times([100]_b-[010]_b)$; $[010]_s=1/2\times([100]_b+[010]_b)$, and $[001]_s=[001]_b$.

[21] R. Feidenhans'l, Surf. Sci. Rep. **10**, 105 (1989).

[22] I. K. Robinson and D. J. Tweet, Rep. Prog. Phys. **55**, 599 (1992).

[23] E. Vlieg, J. Appl. Crystallogr. **30**, 532 (1997).

[24] Two orientations of the reconstructed unit cell on the Cu(001) surface coexist, namely a (4×2) and a 90 degree rotated one, (2×4). This leads to an overlap of most reflections from both domains. For calculating $P(u,v)$, only untwinned reflections can be used.

[25] J. M. Cowley, *Diffraction Physics* (North-Holland Publishing, Amsterdam, 1981).

[26] The unweighted residual (R_u) is defined as $R_u=\Sigma\|I_{obs}|-|I_{calc}\|/\Sigma|I_{obs}|$, where I_{obs} and I_{calc} are the observed and calculated intensities, respectively, and the summation runs over all data points; the goodness-of-fit (GOF) is defined by $\sqrt{[1/(N-P)]\Sigma w(|I_{obs}|-|I_{calc}|)^2}$, where N and P are the number of reflections and refined parameters, respectively, and $w=1/\sigma^2$ is the weighting factor using the standard deviation (σ) as a parameter.

[27] W. Pearson, *A Handbok of Lattice Spacings and Structure of Metals and Alloys* (Pergamon Press, Oxford, 1964).

[28] P. J. Feibelman, Phys. Rev. B **56**, 2175 (1997).

[29] D. Sander and H. Ibach, *Surface Free Energy and Surface Stress*,

Landolt-Börnstein, Numerical Data and Functional Relationships in Science and Technology, New Series, Group III: Condensed Matter, Volume 42, A 2 (Springer, Berlin, 2002), Chap. 4.4, pp. 4.4-1–4.4-49.

[30] D. Meneghetti and S. S. Sidhu, Phys. Rev. **105**, 130 (1957); for a random distributed MnCu alloy, the lattice constant of $Mn_{0.48}Cu_{0.52}$ is 3.75 Å.

[31] M. Wuttig, Y. Gauthier, and S. Blügel, Phys. Rev. Lett. **70**, 3619 (1993).

[32] Y. Tsunoda, N. Oishi, and N. Kunitomi, Physica B & C **119**, 51 (1983); for $Mn_{0.5}Cu_{0.5}$, $c_{11}=110$ GPa, $c_{12}=70$ GPa. $Y/(1-\nu)=c_{11}+c_{12}-2c_{12}^2/c_{11}=91$ GPa.

[33] M. J. Harrison, D. P. Woodruff, and J. Robinson, Surf. Sci. **572**, 309 (2004).